



# Effects of Twist Angle on Rubbing Induced Vibration Responses of Blade

Hui Ma<sup>1,2(✉)</sup>, Tong Yang<sup>1</sup>, Shiyu Liu<sup>1</sup>, Qi Sun<sup>1</sup>, and Bangchun Wen<sup>1</sup>

<sup>1</sup> Northeastern University, Shenyang,  
Liaoning 110819, People's Republic of China  
mahui\_2007@163.com

<sup>2</sup> Key Laboratory of Vibration and Control of Aero-Propulsion System Ministry of Education, Northeastern University, Shenyang,  
Liaoning 110819, People's Republic of China

**Abstract.** In rotating machinery, such as axial-flow compressor, gas turbine and aero-engine, the small clearance between the rotational blade and casing can increase the system efficiency, but may also lead to the rubbing between the blade and casing. The severe rubbing can bring about damages of the blade or casing. In this paper, two mathematical models of blade: a uniform-thickness-shell (UTS) model and a uniform-thickness-twisted-shell (UTTS) model, are established to compare the effects of the blade twist angle on the rubbing-induced vibration responses. The natural characteristics obtained from the two models are compared. Dynamic behaviors obtained from two models considering the combined effects of centrifugal force and aerodynamic force are also compared. Moreover, considering the effects of the misalignment angle and radial misalignment, the transient responses caused by rubbing using the two models are discussed. The results exhibit that the resonance in the radial direction cannot be observed when the blade twist angle is ignored (using UTS model). However, this resonance can be observed using the UTTS model, i.e., taking the influences of twist angle into account.

**Keywords:** Rotating blade · Blade-casing rubbing · Twist angle  
Super-harmonic resonance

## 1 Introduction

In aero engine, the small rotor-stator clearance can improve the system efficiency, but can also bring out the blade-casing rubbing. The rubbing may cause severe vibration of the engine and can decrease the system capability. The rotor-stator rubbing has aroused wide concern, and Jacquet-Richardet et al. [1] and Ma et al. [2] presented a detailed review related to this topic. Generally, the rotor-stator contact (interaction) can be regarded as rubbing in Refs. [3–5], modal interaction in Refs. [6–8] and whirl and whip in Ref. [9]. For the sake of obtaining a deep understanding of the dynamic characteristics during rubbing, some theoretical and experimental researches [3, 4, 10–13] were presented, and some numerical methods are proposed by Batailly et al. [14] and Parent et al. [15].

According to the different requirement of simulation modeling, the blade can be regarded as beam, thin plate and three-dimensional solid model in many studies. The

three-dimensional blade is simplified as a beam model [3, 4, 8]. It is clear that the beam model cannot accurately analyze the vibration response in the chord wise direction. For improving the precision of the beam model, the plate models are also widely adopted [11]. Adopting the thin shell theory, Sun et al. [16] established a new dynamic model of a rotational blade with stagger angles, and analyzed the dynamic characteristics of the blade systems. Yoo et al. [17] proposed a new method to carry out the modal analysis of a rotational cantilever plate, and discussed the modal behaviors of the plate under different structural and load parameters, such as the aspect ratios and the angular speeds. Sinha and Zylka [18] developed a dynamic model using thin shell theory to analyze the transverse vibration of a rotational blade.

Many researchers adopted three dimensional finite element models due to their accuracy, especially for complicated structures. A three-dimensional finite element model for a partial blade-disk with dovetail is established, and the dynamic behaviors of the blade and contact characteristics of dovetail are analyzed in Ref. [12]. It is obvious that the numerical simulation is time-consuming adopting a three-dimensional finite element model with large sizes.

From the above literatures, it can be observed that the dynamic characteristics of blade considering the effects of twist angle were investigated, however, the influences of blade twist angle on the responses caused by rubbing are not involved. In order to make up for this deficiency, in this paper, two finite element models of blade, i.e., uniform-thickness shell (UTS), and uniform-thickness-twisted shell (UTTS) models, are established to compare the influences of twist angles of blade on the system vibration responses during rubbing.

## 2 Finite Element Models of Blade and Blade-Casing Rubbing Model

### 2.1 Finite Element Model of Blade

For the UTS model, the simulation parameters are shown in Table 1. Compared with the UTS model, the UTTS model considers the effects of twist angle of the blade  $\gamma_L$  (see Fig. 1a,  $\gamma_L = 10^\circ$  in this paper), and other parameters are all the same as those of the UTS model. It should be noted that the geometry of the UTTS model is shaped by extruding the rectangle along the  $Z$  axis with a constant rate  $\gamma'$  of the twist angle, such that the twist angle along the  $Z$  axis can be expressed as  $\gamma(Z) = \gamma' Z = \frac{\gamma_L}{L} \times Z$ . The UTTS is built by 9 mid-curves related to the profiles, as shown in Fig. 1b, where the thickness  $h$  is calculated by the blade surface data. The detailed modelling process can be found in Ref. [19].

**Table 1.** Blade simulation parameters

Material parameters	Values	Parameters of disk and blade	Values
Young's modulus $E$ (GPa)	125	Radius of the disk $R_d$ (mm)	216.52
Density $\rho$ (kg/m <sup>3</sup> )	4370	Blade length $L$ (mm)	88.6
Poisson's ratio $\nu$	0.3	Blade width $b$ (mm)	56.7
		Stagger angle $\beta_2$ ( $^\circ$ )	35.32

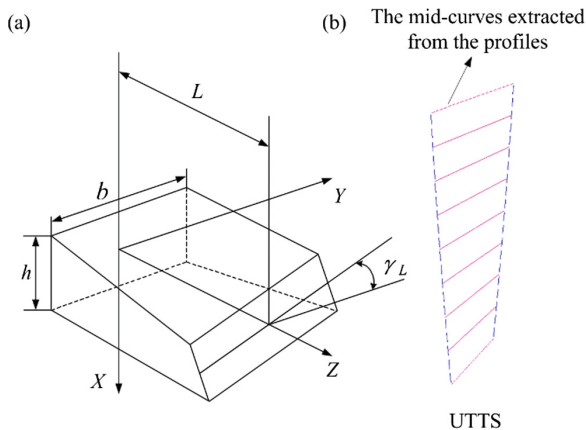


**Fig. 1.** Schematic diagram of the geometry: (a) schematic diagram of twist angle, (b) modeling schematic diagram for UTTS

Based on ANSYS, two finite element models are established, where the UTS and the UTTS FE models are established by Shell181 elements. For the UTS and the UTTS models, 20 elements (21 nodes) are divided on the blade-tip. It is worth noting that in the UTS and the UTTS model, the blade width (chord length) is set as the distance between the leading edge and trailing edge (see Fig. 2).

Note: LE denotes leading edge; TE denotes trailing edge

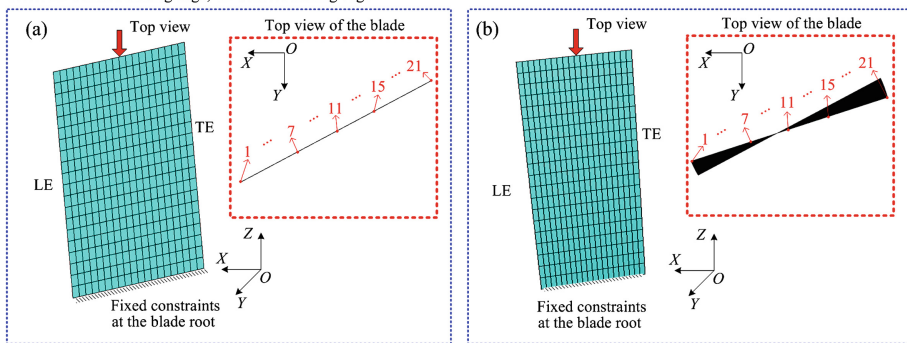


**Fig. 2.** Finite element models of blades: (a) UTS model, (b) UTTS model

The motion equations of the blade are

$$\mathbf{M}\ddot{\mathbf{u}} + [\mathbf{D} + \mathbf{G}(\Omega)]\dot{\mathbf{u}} + [\mathbf{K}_e + \mathbf{K}_c(\Omega) + \mathbf{K}_s(\Omega) + \mathbf{K}_{acc}(\dot{\Omega})]\mathbf{u} = \mathbf{f} \quad (1)$$

The detailed introduction about  $\mathbf{M}$ ,  $\mathbf{D}$ ,  $\mathbf{G}(\Omega)$ ,  $\mathbf{K}_e$ ,  $\mathbf{K}_c(\Omega)$ ,  $\mathbf{K}_s(\Omega)$ ,  $\mathbf{K}_{acc}(\dot{\Omega})$ ,  $\mathbf{u}$  and  $\mathbf{f}$  can be found in Ref. [19].

### 2.2 Blade-Casing Rubbing Model

Considering the effects of angle misalignment  $\beta_1$  and radial misalignment, blade-casing rubbing model is established (see Fig. 3). The detailed introduction of the showed parameters can be found in Ref. [19].

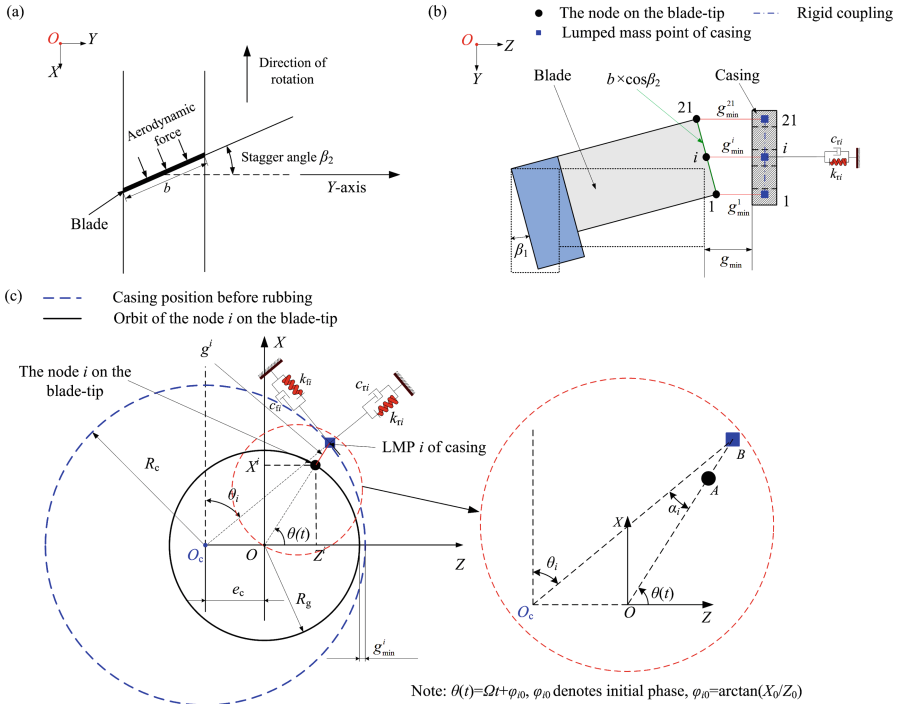


**Fig. 3.** (a) blade top view (b) blade-casing clearance (c) the clearance between blade-tip node  $i$  and LMP  $i$  of casing.

The clearance  $g_{rub}^i$  can be written as

$$g_{rub}^i = g^i - u_{Zb}^i + u_{Zc}^i \tag{2}$$

where  $u_{Zb}^i$  and  $u_{Zc}^i$  are radial displacements of blade-tip node  $i$  and LMP  $i$  of the casing, respectively. For the UTS and the UTTS models,  $i = 1, 2, \dots, 21$ . Here, it should be noted that the influences of the bending vibration of the casing on  $g_{rub}^i$  are not considered.  $g^i$  can be written as

$$g^i = \begin{cases} R_c \sin(\pi/2 - \theta_i(t)) / \sin \theta(t) - R_g & \theta(t) \neq n\pi \\ g_{min}^i & \theta(t) = 2n\pi \\ 2R_c - 2R_g - g_{min}^i & \theta(t) = (2n + 1)\pi \end{cases}$$

where  $n$  denotes positive integer;  $R_c = l_{O,B}$ ;  $\theta_i(t) = \pi/2 - \theta(t) + \alpha_i(t)$  (see Fig. 3c),  $\varphi_{i0} = \arctan(Z_0^i/X_0^i)$ , here,  $Z_0^i$  and  $X_0^i$  denote the initial  $Z$  and  $X$  coordinates of the node  $i$  on the blade-tip.  $\alpha_i(t)$  can be written as

$$\alpha_i(t) = \arcsin((R_c - g_{\min}^i - R_g) \sin \theta(t)/R_c) \tag{4}$$

where  $g_{\min}^i = g_{\min 1} + (21 - i) \times b \times \cos \beta_2/20 \times \sin \beta_1$ .  $g_{\min 1}$  is

$$g_{\min 1} = g_{\min} - (R_g \cos \beta_1 + b \cos \beta_2 \times \sin \beta_1 - R_g) \tag{5}$$

The penetration depth  $\delta_i$  of the blade-tip node  $i$  is

$$\delta_i = \begin{cases} -g_{\text{rub}}^i & g_{\text{rub}}^i < 0 \\ 0 & g_{\text{rub}}^i \geq 0 \end{cases} \tag{6}$$

The equivalent normal rubbing force  $F_{Zb}^i$  of blade-tip node  $i$  is

$$F_{Zb}^i = f_n \frac{\delta_i}{\delta} \tag{7}$$

where  $\delta$  denotes the penetration depth sum of each blade-tip node, and it can be written as:

$$\delta = \sum_{i=1}^n \delta_i \tag{8}$$

Assuming that the casing stiffness is linear [19], the rubbing force is

$$f_{\text{elastic}} = k_{ri} u_c, \tag{9}$$

where  $k_{ri}$  and  $u_c$  are the equivalent casing stiffness and the casing radial displacement. The force balance relation is shown the following expression.

$$f_n = f_{\text{elastic}}, \tag{10}$$

The tangential rubbing force of blade-tip node  $i$  is

$$F_{Xb}^i = \mu F_{Zb}^i \tag{11}$$

where  $\mu$  is the coefficient of friction.

### 3 Dynamic Characteristics of Two Blade Models Without Rubbing

The section will firstly analyze the natural characteristics of rotational blade adopting two finite element models. Taking the effects of the stress stiffening, spin softening and Coriolis force into account, the first two natural frequencies and their mode shapes are

displayed in Figs. 4 and 5. In the figure,  $10\Omega$  represents the aerodynamic force frequency. The intersections of  $10\Omega$  line and the first natural frequency are defined as critical speeds, and they are 3999 RPM for UTS model and 3998 RPM for UTTS model, respectively. The first two natural frequencies are also shown in Table 2, which shows a light error (smaller than 0.4%) between natural frequencies obtained from two models.

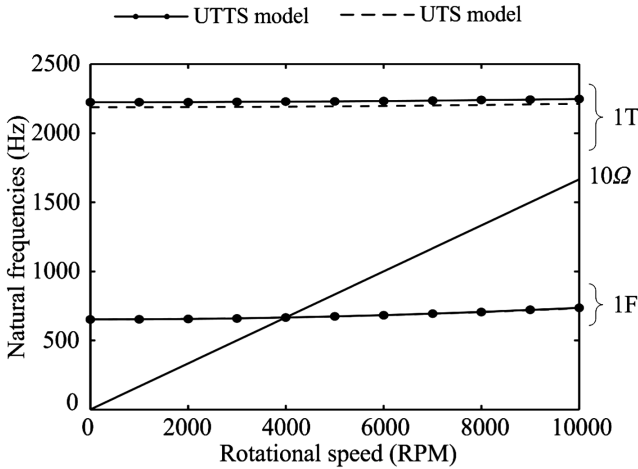


Fig. 4. Natural frequencies of the blade

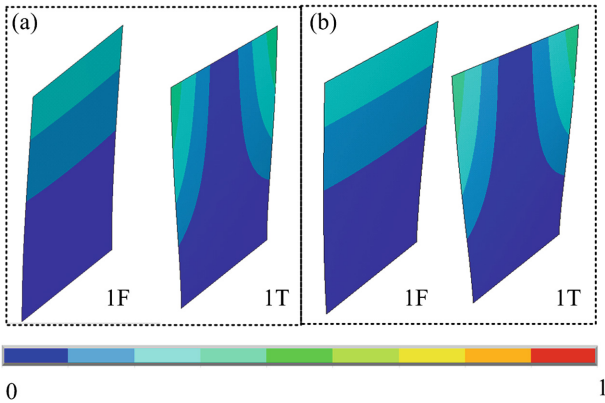


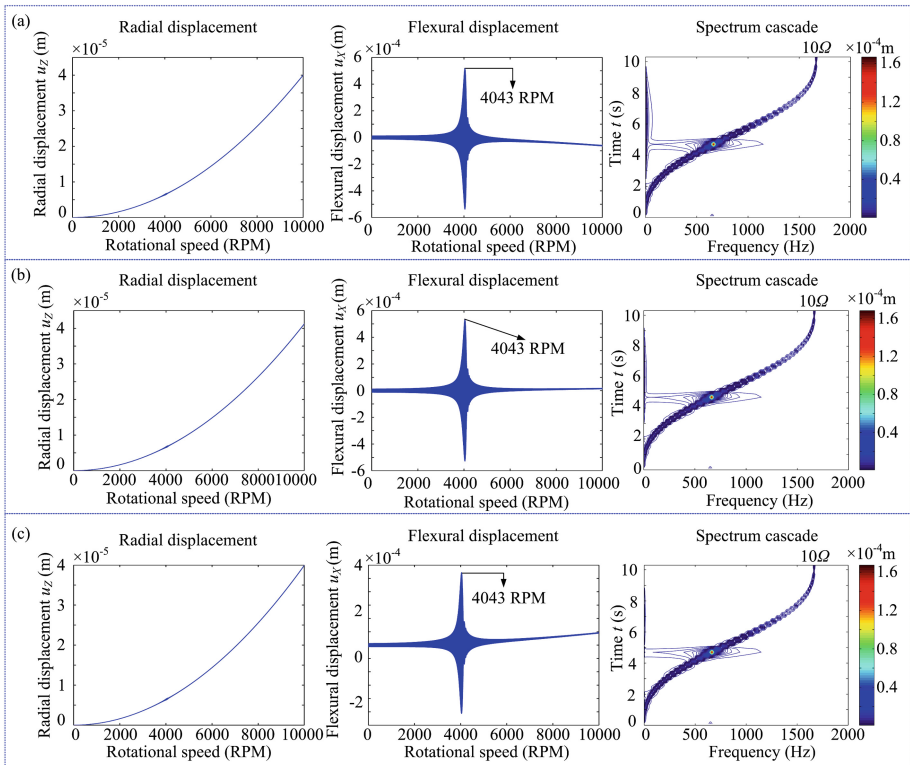
Fig. 5. Mode shapes obtained from two finite models at rest: (a) UTS model, (b) UTTS model

Comparison on the vibration responses of different blade-tip nodes are displayed in Figs. 6 and 7. In these figures, the nodes 1, 11, and 21 are used to describe the vibration of the leading edge, the blade-tip middle point and trailing edge.

**Table 2.** Natural frequencies obtained from two finite element models

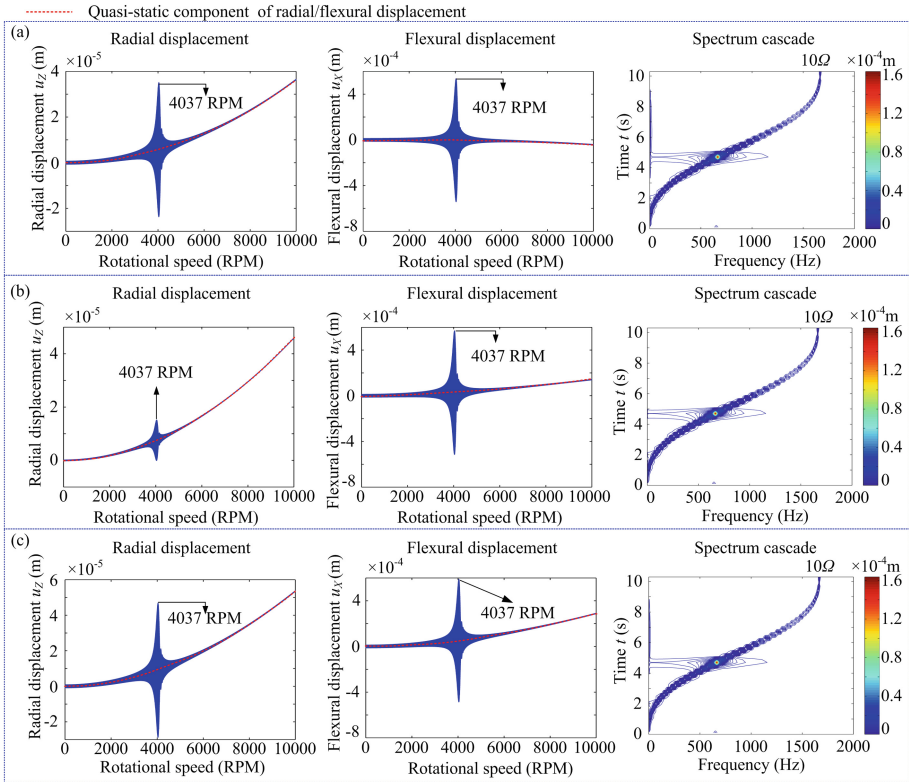
Mode	Models	Rotational speeds (RPM)					
		0	2000	4000	6000	8000	10000
1F	UTS (Hz)	652.875	656.292	666.436	682.997	705.508	733.402
	UTTS (Hz)	652.197	655.871	666.411	683.741	707.269	736.384
1T	UTS (Hz)	2188.227	2189.248	2192.311	2197.404	2204.514	2213.620
	UTTS (Hz)	2232.554	2233.543	2236.509	2241.441	2248.328	2257.149

The run-up response in the radial direction shows that for the UTS model, the radial displacements include only a static component due to the centrifugal force (see radial displacement in Fig. 6). For the UTTS models, the radial displacements include two distinct components: static component related to the centrifugal force and a high frequency component caused by aerodynamic force. Moreover, for the UTTS model, the radial-direction resonance peaks (the first order resonance) can be observed because the blade twist angles have an effect on the radial vibration (see Fig. 7).



Note: The relationship between rotational speed  $\Omega$  (RPM) and time  $t$  (s) can be expressed as:  $\Omega(t) = \frac{3000}{\pi}t - \frac{5000}{\pi} \sin(\frac{3}{5}t)$

**Fig. 6.** Vibration responses of blade-tip nodes without rubbing (UTS model): (a) node 1, (b) node 11, (c) node 21.



Note: The relationship between rotational speed  $\Omega$  (RPM) and time  $t$  (s) can be expressed as:  $\Omega(t) = \frac{3000}{\pi}t - \frac{5000}{\pi}\sin(\frac{3}{5}t)$

**Fig. 7.** Vibration responses of blade-tip nodes without rubbing (UTTS model): (a) node 1, (b) node 11, (c) node 21.

The flexural displacement also includes the static component and the high frequency component. The static components have different change trend for different blade-tip positions (see Figs. 6 and 7).

### 4 Vibration Responses of Blade and Casing Under Rubbing

When the rotor speeds up from  $\Omega_0$  to  $\Omega_{end}$ , vibration responses of the blade-tip nodes (node 21) and casing based on two finite element models, are displayed in Figs. 8 and 9.

Except for the aerodynamic loads induced primary resonances, many rubbing induced super-harmonic resonances also appear when the multiple of the rotating speed is close to the blade natural frequency. For example, the resonance peaks obtained from the UTS model can be observed at 6994 RPM (see Fig. 8b) which are excited due to six times of rotating frequencies  $6\Omega$  ( $6\Omega = f_{n1}$  Hz,  $f_{n1}$  denotes the first natural frequency of blade) and five times of rotating frequencies  $5\Omega$  ( $5\Omega = f_{n1}$  Hz) approaching  $f_{n1}$ . More super-harmonic resonance peaks can be observed when using the UTTS



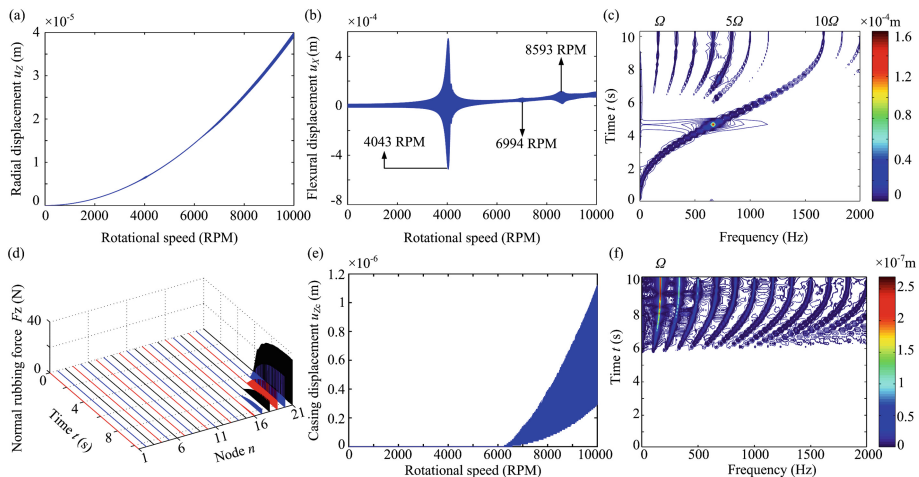


**Fig. 8.** Vibration responses of node 21 (UTS model): (a) radial displacement, (b) flexural displacement, (c) spectrum cascade, (d) normal rubbing forces, (e) radial displacement of the casing, (f) spectrum cascade of the casing

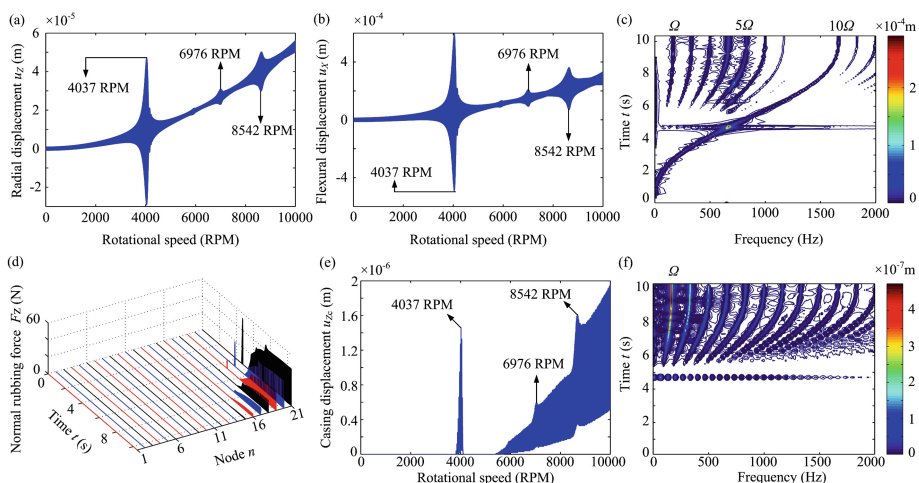


**Fig. 9.** Vibration responses on node 21 (UTTS model): (a) radial displacement, (b) flexural displacement, (c) spectrum cascade, (d) normal rubbing forces, (e) radial displacement of the casing, (f) spectrum cascade of the casing

model than those of the UTS model, and the super-harmonic resonance phenomena become even more abundant, compared with the UTTS model.

For the UTTS model, the first blade-tip rubbing occurs near 4037 RPM because the radial-direction resonance peak of the blade appears at 4037 RPM under the action of aerodynamic and centrifugal loads. With the increasing rotational speed, the radial elongation of the blade-tip increases, the rubbing appears again (see Fig. 9d).

The time history, frequency spectra and displacement nephograms obtained from the speed-up process (near  $5\Omega = f_{n1}$  Hz) are discussed (see Figs. 10, 11, 12 and 13). It should be noted that in the time-domain waveforms (see Figs. 10a and 12a), the left-hand vertical ordinate axis (blue line) shows the flexural displacement of the node 21, and the right-hand vertical ordinate axis (green line) shows the normal rubbing force. The time segments for frequency spectra are in the interval of [7.3215 s, 7.4685 s] for the UTS and the UTTS models. The displacement nephograms of the blade at four typical moments A, B, C and D (see Figs. 10a and 12a) are shown in Figs. 11 and 13. Compared the vibration obtained from the UTS and the UTTS models, it is obvious that the vibration increases sharply due to the effect of the twist-shape of the blade (see Figs. 10 and 12). The results also show that the vibration response is predominant near  $f_{n1}$  in comparison with that near  $f_{n2}$ , as shown in Figs. 10b and 12b. It should be noted that for the UTS and the UTTS models,  $15\Omega \approx f_{n2}$ . In the displacement nephograms, the bending-torsion coupled vibrations of blade can be observed under  $5\Omega \approx f_{n1}$  (see Figs. 11a and 13a) because the twist angle leads to the stiffness coupling in radial and flexural directions.

Note: A, B, C and D denote four typical moments

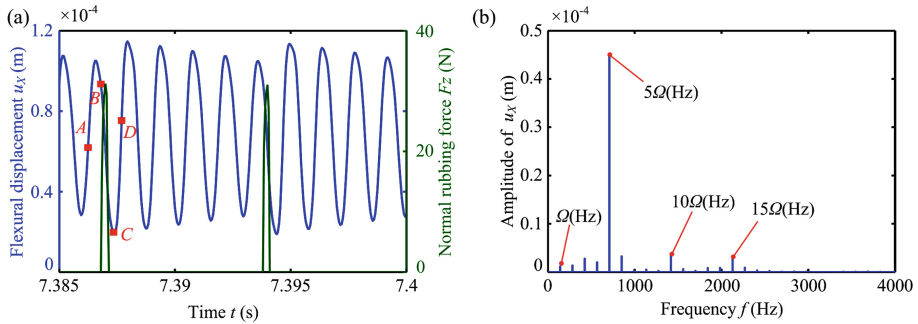


**Fig. 10.** Vibration responses of the node 21 near 8593 RPM (UTS model): (a) flexural displacement waveform, (b) frequency spectrum

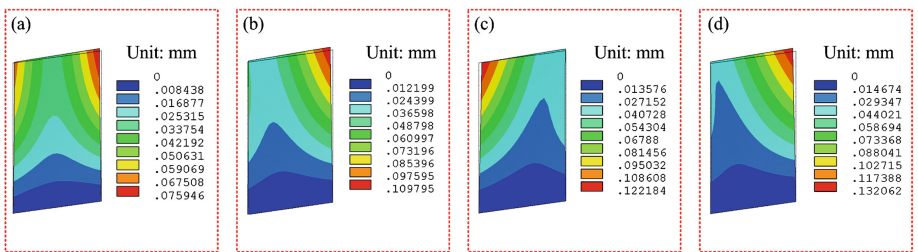


**Fig. 11.** Displacement nephograms near 8593 RPM (UTS model): (a) moment A, (b) moment B, (c) moment C, (d) moment D

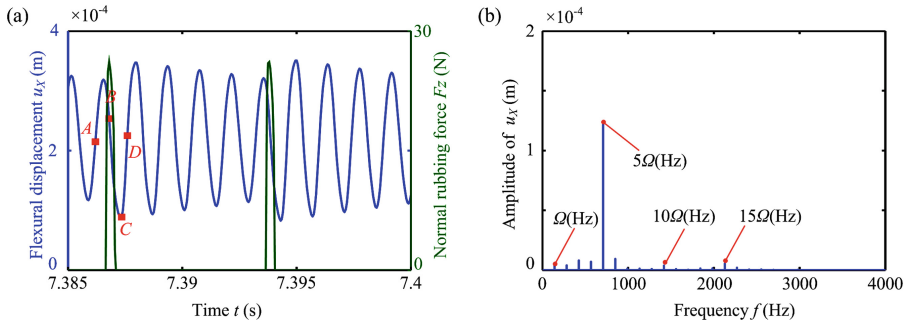


**Fig. 12.** Vibration responses of the node 21 near 8542 RPM (UTTS model): (a) flexural displacement waveform, (b) frequency spectrum

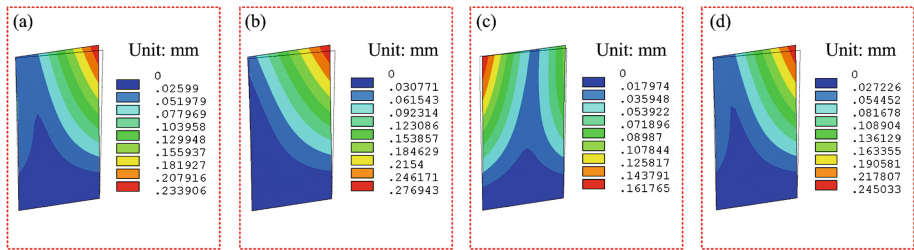


**Fig. 13.** Displacement nephograms near 8542 RPM (UTTS model): (a) moment A, (b) moment B, (c) moment C, (d) moment D

## 5 Conclusions

In this paper, the influences of blade twist angle on the vibration responses caused by rubbing are analyzed using two finite element models, i.e., the uniform-thickness shell (UTS) and uniform-thickness-twisted shell (UTTS) models. The casing is simulated by a lumped mass with spring and damping. By rubbing force to couple the blade can casing models, the blade-casing rubbing phenomena are simulated. Mainly conclusions are listed as follows:

The simulated results show that the twist angle can not affect the rubbing induced super-harmonic resonance phenomena in flexural direction. The vibration response is predominant near the first dynamic frequency compared with that near the second dynamic frequency. The rubbing can excite the blade bending-torsional coupled vibration.

The twist angle affects the resonance in the radial direction, and this resonance can be observed for the blade with twist angle. In addition, the twist angle also affects the active sets of rubbing nodes due to different blade-tip deformations.

**Acknowledgment.** This project is supported by the China Natural Science Funds (NSFC, Grant no. 11772089) and the Fundamental Research Funds for the Central Universities (Grant nos. N160313004 and N160312001).

## References

1. Jacquet-Richardet, G., Torkhani, M., Cartraud, P., et al.: Rotor to stator contacts in turbomachines. *Rev. Appl. Mech. Syst. Signal Process.* **40**, 401–420 (2013)
2. Ma, H., Yin, F.L., Guo, Y.Z., Tai, X.Y., Wen, B.C.: A review on dynamic characteristics of blade-casing rubbing. *Nonlinear Dyn.* **84**(2), 437–472 (2016)
3. Ma, H., Yin, F.L., Wu, Z.Y., et al.: Nonlinear vibration response analysis of a rotor-blade system with blade-tip rubbing. *Nonlinear Dyn.* **84**(3), 1225–1258 (2016)
4. Sinha, S.K.: Non-linear dynamic response of a rotating radial Timoshenko beam with periodic pulse loading at the free-end. *Int. J. Non-Linear Mech.* **40**(1), 113–149 (2005)
5. Turner, K.E., Dunn, M., Padova, C.: Airfoil deflection characteristics during rub events. *J. Turbomachinery* **134**(1), 011018-1–011018-8 (2012)
6. Schmiechen, P.: Travelling wave speed coincidence. Ph.D. thesis, Imperial College of Science, Technology and Medicine—University of London (1997)
7. Legrand, M., Pierre, C., Cartraud, P., Lombard, J.P.: Two-dimensional modeling of an aircraft engine structural bladed disk-casing modal interaction. *J. Sound Vib.* **319**(1–2), 366–391 (2009)
8. Batailly, A., Legrand, M., Cartraud, P., et al.: Assessment of reduced models for the detection of modal interaction through rotor stator contacts. *J. Sound Vib.* **329**(26), 5546–5562 (2010)
9. Childs, D.W., Bhattacharya, A.: Prediction of dry-friction whirl and whip between a rotor and a stator. *J. Vib. Acoust.* **129**(3), 355–362 (2007)
10. Sinha, S.K.: Dynamic characteristics of a flexible bladed-rotor with Coulomb damping due to tip-rub. *J. Sound Vib.* **273**(4–5), 875–919 (2004)
11. Yuan, H.Q., Kou, H.J.: Contact-impact analysis of a rotating geometric nonlinear plate under thermal shock. *J. Eng. Math.* **90**(1), 119–140 (2015)
12. Ma, H., Wang, D., Tai, X.Y., Wen, B.C.: Vibration response analysis of blade-disk dovetail structure under blade tip rubbing condition. *J. Vib. Control* **23**(2), 252–271 (2017)
13. Almeida, P., Gibert, C., Thouverez, F., et al.: Experimental analysis of dynamic interaction between a centrifugal compressor and its casing. *J. Turbomachinery* **137**(3), 031008-1–031008-10 (2014)
14. Batailly, A., Legrand, M., Pierre, C.: Full three-dimensional rotor/stator interaction simulations in aircraft engines with time-dependent angular speed. *J. Eng. Gas Turbines Power* **139**(3), 031202-1–031202-7 (2017)
15. Parent, M.O., Thouverez, F., Chevillot, F.: Whole engine interaction in a bladed rotor-to-stator contact. In: *ASME Turbo Expo 2014: Turbine Technical Conference and Exposition*. American Society of Mechanical Engineers, 2014
16. Sun, J., Arteaga, I.L., Kari, L.: General shell model for a rotating pretwisted blade. *J. Sound Vib.* **332**(22), 5804–5820 (2013)
17. Yoo, H.H., Kim, S.K., Inman, D.J.: Modal analysis of rotating composite cantilever plates. *J. Sound Vib.* **258**(2), 233–246 (2002)
18. Sinha, S.K., Zylka, R.P.: Vibration analysis of composite airfoil blade using orthotropic thin shell bending theory. *Int. J. Mech. Sci.* **121**, 90–105 (2017)
19. Sun, Q., Ma, H., Zhu, Y.P., et al.: Comparison of rubbing induced vibration responses using varying-thickness-twisted shell and solid-element blade models. *Mech. Syst. Sig. Process.* **108**, 1–20 (2018)